Acta Crystallographica Section D
Biological Crystallography
ISSN 0907-4449

Direct metal recognition by guanine nucleotide-exchange factor in the initial step of the exchange reaction

Tamami Uejima,[a]*‡ Kentaro Ihara,[a]*‡ Mariko Sunada,[b] Masato Kawasaki,[a] Takashi Ueda,[b] Ryuichi Kato,[a] Akihiko Nakano[c] and Soichi Wakatsuki[a]*

[a]Structural Biology Research Center, Institute of Materials Structure Science, High Energy Accelerator Research Organization, 1-1 Oho, Tsukuba, Ibaraki 305-0801, Japan, [b]Laboratory of Developmental Cell Biology, Department of Biological Sciences, Graduate School of Science, University of Tokyo, Tokyo 113-0033, Japan, and [c]Molecular Membrane Biology Laboratory, RIKEN Advanced Science Institute, Saitama 351-0198, Japan

‡ These authors contributed equally to this work.

Correspondence e-mail: tamami.uejima@kek.jp, kentaro.ihara@kek.jp, soichi.wakatsuki@kek.jp

Received 26 September 2012
Accepted 17 November 2012

PDB Reference: ARA7-GDP-Ca^{2+}–VPS9a, 4g01

Rab small GTPases regulate vesicle transport in eukaryotes by interacting with various effectors. Guanine nucleotide-exchange factor (GEF) catalyzes the transition from inactive GDP-bound Rab to active GTP-bound Rab. The existence of several GDP-bound intermediates containing the *Arabidopsis thaliana* Rab5 homologue ARA7 and the GEF VPS9a prior to the formation of a nucleotide-free binary complex has been proposed [Uejima *et al.* (2010), *J. Biol. Chem.* **285**, 36689–36697]. During this process, VPS9a directly interacts with the β-phosphate of GDP and the P-loop lysine of ARA7 *via* a catalytically important aspartate finger, which promotes the release of GDP from ARA7. However, it is unclear how VPS9a removes Mg^{2+} from ARA7 before forming the GDP-bound ternary complex. Here, the structure of the ARA7-GDP-Ca^{2+}–VPS9a complex is reported, in which the aspartate finger directly coordinates the divalent metal ion. Ca^{2+} is bound to the canonical Mg^{2+}-binding site, coordinated by the β-phosphate of GDP and the P-loop serine of ARA7. Unexpectedly, Ca^{2+} is further coordinated by the aspartate finger and the main chain of VPS9a. This structure may represent the earliest intermediate step in the GEF-catalyzed nucleotide-exchange reaction of ARA7 before the metal-free GDP-bound intermediates are created.

1. Introduction

Small GTPases serve as molecular switches, alternating between active and inactive states in terms of binding to target proteins (effectors). GTP-bound small GTPases play a range of biological roles by interacting with various effectors. GTP is hydrolyzed to GDP *via* the intrinsic GTPase activity of the enzyme, which is promoted by GTPase-activating proteins (GAPs). To reactivate GDP-bound small GTPases, GEF first removes the Mg^{2+} from the GTPase to destabilize GDP binding (Sprang & Coleman, 1998; Cherfils & Chardin, 1999; Stenmark, 2009; Itzen & Goody, 2011).

Rab small GTPases regulate vesicular transport in eukaryotes (Barr & Lambright, 2010; Zerial & McBride, 2001), including plants (Ueda & Nakano, 2002). The model plant *Arabidopsis thaliana* has three homologues of Rab5 named ARA7, ARA6 and RHA1 (Ueda *et al.*, 2001). In *A. thaliana*, the exchange of GDP for GTP in these Rab5s is catalyzed by its sole GEF, VPS9a (Horiuchi *et al.*, 1997; Goh *et al.*, 2007).

The mechanism of Mg^{2+} removal and the subsequent release of GDP from GTPases has been well established in several GTPase–GEF systems including Ras and Rho family GTPases, such as Ras–Sos (Boriack-Sjodin *et al.*, 1998), Rac1–Tiam1 (Worthylake *et al.*, 2000), Ran–RCC1 (Renault *et al.*, 2001) and Cdc42–SpoE (Buchwald *et al.*, 2002). Although

these GTPase–GEF complexes were crystallized as the nucleotide-free forms, the structures revealed that a GEF-mediated conformational change in the GTPase switch II region results in a conserved alanine residue in the switch II region sterically interfering with Mg^{2+} binding (Boriack-Sjodin *et al.*, 1998; Worthylake *et al.*, 2000). Furthermore, the conformational change creates an ionic interaction between a conserved P-loop lysine and a glutamate in switch II which prevents the P-loop lysine from interacting with the β-phosphate of GDP and leads to GDP release.

Nucleotide-free GTPase–GEF complexes are stable, whereas the complexes are destabilized, in the presence of Mg^{2+} and nucleotides. Thus, GTPase–GEF complexes have usually been prepared in the absence of Mg^{2+} and nucleotides. The plant Rho Rop4, however, was crystallized with a GEF (PRONE) and GDP (Thomas *et al.*, 2007). The structure of nucleotide-bound Rop4–PRONE represented an intermediate state after dissociation of Mg^{2+} and confirmed the mechanisms of nucleotide exchange that had been proposed based on the nucleotide-free GTPase–GEF complex structures. A more recent report has detailed the structure of nucleotide-bound Cdc42–DOCK9 (Yang *et al.*, 2009). Unlike the common GTPase–GEF mechanism, the conserved switch II alanine of Cdc42–DOCK9 does not interfere with Mg^{2+} binding. Instead, a valine of DOCK9 that is conserved in DOCK proteins, termed the nucleotide sensor, inserts into the metal-binding site and directly occludes Mg^{2+} (Yang *et al.*, 2009).

For Arf family GTPases, nucleotide exchange is stimulated by the Sec7-domain-containing family of proteins, which carry an invariant glutamate residue named the 'glutamate finger' (Goldberg, 1998). In the Arf1–Sec7 complex, introducing an abortive inhibitor between the interface allowed GDP and Mg^{2+} to bind (Renault *et al.*, 2003; Mossessova *et al.*, 2003), whereas replacing the glutamate finger of Sec7 by a lysine residue led to the binding of GDP but not Mg^{2+} (Renault *et al.*, 2003).

Among the Rab family GTPases, a nucleotide-free structure of Rab21–Rabex-5 has been reported (Delprato & Lambright, 2007). As a GEF for Rab5, Rab21 and Rab22, Rabex-5 contains a catalytic Vps9 domain with an aspartate finger that is analogous to the glutamate finger in Sec7 (Goldberg, 1998; Delprato & Lambright, 2007; Béraud-Dufour *et al.*, 1998). We have described nucleotide-free and nucleotide-bound structures of ARA7–VPS9a, which is the Rab5–Vps9 homologue from *A. thaliana* (Uejima *et al.*, 2010). The structure of ARA7-GDP–VPS9a showed a direct interaction between the β-phosphate of GDP and Asp185 (aspartate finger) of VPS9a. Movement of the conserved Lys23 in the P-loop of ARA7 and Asp185 of VPS9a leads to dissociation of GDP from the GTPase. In intermediates other than the GDP-bound complex, Lys23 in the P-loop swings from the β-phosphate towards Asp65 in the switch II region of ARA7, resulting in loss of the anchor between GDP and the GTPase (Uejima *et al.*, 2010). This process should correspond to the general GDP-release mechanism catalyzed by GEF, in which movement of the P-loop lysine away from GDP is critical. However, the mechanism by which the divalent metal bound to ARA7 and GDP is removed by VPS9a before the ternary ARA7-GDP–VPS9a complex forms is unclear. This led us to determine the structure of a complex containing a nucleotide and a divalent cation. Here, we report the crystal structure of ARA7-GDP-Ca^{2+}–VPS9a, which reveals that the metal ion directly interacts with the aspartate finger of VPS9a.

Table 1
Crystallographic data and refinement statistics of the ARA7-GDP-Ca^{2+}–VPS9a complex.

Values in parentheses are for the highest resolution bin.

Data collection and processing	
Beamline	NW12A, PF-AR
Wavelength (Å)	1.0000
Detector	ADSC Q210
Crystal-to-detector distance (mm)	189.60
Rotation range per image (°)	0.5
Total rotation range (°)	180.0
Unit-cell parameters (Å, °)	a = 68.3, b = 76.1, c = 81.8, $\alpha = \beta = \gamma$ = 90.0
Space group	$P2_12_12_1$
Solvent content (%)	44
Processed resolution (Å)	2.2 (2.24–2.20)
R_{merge}† (%)	13.0 (69.1)
Completeness (%)	100.0 (99.9)
Average multiplicity	7.2 (7.0)
Average $I/\sigma(I)$	15.8 (2.8)
Mosaicity (°)	0.6–1.1
Refinement and validation	
Resolution (Å)	2.20 (2.26–2.20)
R_{work}‡ (%)	19.8 (22.0)
R_{free}§ (%)	27.3 (29.2)
R.m.s.d., bond lengths (Å)	0.013
R.m.s.d., bond angles (°)	1.4
Wilson B value (Å^2)	29.4
Overall $\langle B\rangle$ (Å^2)	32.1
$\langle B\rangle$, ARA7 (Å^2)	33.4
$\langle B\rangle$, VPS9a (Å^2)	30.6
$\langle B\rangle$, nucleotides (Å^2)	27.7
$\langle B\rangle$, nucleotide-bound metals (Å^2)	24.6
$\langle B\rangle$, waters (Å^2)	36.1
Residues (ARA7/VPS9a)	8–172/26–262
No. of nucleotides	1
No. of nucleotide-bound metals	1
No. of waters	261

† $R_{merge} = 100 \times \sum_{hkl}\sum_i |I_i(hkl) - \langle I(hkl)\rangle| / \sum_{hkl}\sum_i I_i(hkl)$, where $\langle I(hkl)\rangle$ is the mean intensity of symmetry-related reflections. ‡ $R_{work} = 100 \times \sum_{hkl} \big||F_{obs}| - |F_{calc}|\big| / \sum_{hkl} |F_{obs}|$, where F_{obs} and F_{calc} are observed and calculated reflections. § A randomly chosen 5% of reflections were used for the calculation of R_{free}.

2. Materials and methods

2.1. Proteins

ARA7cd1 (residues 1–179 of ARA7 plus 12 additional amino-acid residues encoded by the expression vector (see Uejima *et al.*, 2010) and VPS9a (residues 1–265) were produced as glutathione S-transferase (GST) fusion proteins using the pGEX4T1 expression vector (GE Healthcare) in *Escherichia coli* strains DH5α and Rosetta-gami(DE3)pLysS (Novagen), respectively. The proteins were purified using glutathione Sepharose resin (GE Healthcare) in a buffer consisting of 50 m*M* Tris–HCl pH 7.4, 50 m*M* NaCl, 1 m*M* EDTA. For crystallization, the GST moiety was cleaved using thrombin. GDP-bound ARA7 was purified in the absence of

Table 2
Kinetic constants for the interaction between ARA7 and VPS9a.

(*a*) No nucleotide.

	K_d (*M*)	k_a (M^{-1} s^{-1})	k_d (s^{-1})
EDTA	2.6×10^{-7}	4.8×10^{3}	1.2×10^{-3}
1 m*M* $MgCl_2$	2.4×10^{-7}	5.9×10^{3}	1.4×10^{-3}
1 m*M* $CaCl_2$	2.0×10^{-7}	7.0×10^{3}	1.4×10^{-3}

(*b*) GppNHp.

	K_d (*M*)	k_a (M^{-1} s^{-1})	k_d (s^{-1})
EDTA	3.5×10^{-7}	4.5×10^{3}	1.6×10^{-3}
1 m*M* $MgCl_2$	†	†	†
1 m*M* $CaCl_2$	5.6×10^{-6}	1.4×10^{3}	7.5×10^{-3}

(*c*) GDP.

	K_d (*M*)	k_a (M^{-1} s^{-1})	k_d (s^{-1})
EDTA	6.1×10^{-6}	8.0×10^{3}	4.9×10^{-2}
1 m*M* $MgCl_2$	†	†	†
1 m*M* $CaCl_2$	3.4×10^{-6}	1.9×10^{4}	6.3×10^{-2}

† No interaction was observed.

Mg^{2+} and of additional GDP. After mixing ARA7-GDP and VPS9a, nucleotide-free ARA7–VPS9a was separated using a Mono Q anion-exchange column (GE Healthcare) in a buffer consisting of 50 m*M* Tris–HCl pH 7.4, 1 m*M* EDTA with a linear gradient of NaCl from 0 to 0.7 *M*, followed by size-exclusion chromatography on a Superdex 200 10/300 GL column (GE Healthcare) in a solution consisting of 10 m*M* Tris–HCl pH 7.4, 50 m*M* NaCl, 1 m*M* EDTA.

2.2. Crystallography

A crystal of ARA7-GDP-Ca^{2+}–VPS9a was obtained using a hanging-drop setup by mixing 1 µl 1 m*M* GDP and 2 mg ml^{-1} nucleotide-free ARA7–VPS9a with 1 µl reservoir solution consisting of 20%(*v*/*v*) PEG 3350, 200 m*M* calcium acetate pH 6.5. The mixture was equilibrated against 200 µl of the reservoir solution *via* vapour diffusion. Diffraction data were collected on beamline AR-NW12A at the Photon Factory, KEK, Tsukuba, Japan and were processed using *HKL*-2000 (Otwinowski & Minor, 1997). The initial phase set of the data was determined based on molecular replacement with *MOLREP* (Vagin & Teplyakov, 2010) in the *CCP*4 suite (Winn *et al.*, 2011), which unambiguously found a solution using the structure of the nucleotide-free ARA7-GDP–VPS9a complex (PDB entry 2efc; Uejima *et al.*, 2010) as a search model followed by iterative model refinement using *REFMAC*5 (Murshudov *et al.*, 2011) and *Coot* (Emsley & Cowtan, 2004). Structural figures were prepared using *RasMol* (Sayle & Milner-White, 1995), *MolScript* (Kraulis, 1991), *Raster3D* (Merritt & Murphy, 1994) and *PyMOL* (Schrödinger; http://www.pymol.org). The stereochemical quality and secondary structure of the model were checked using *Coot* and *PROCHECK* (Laskowski *et al.*, 1993); no main-chain torsion angles were located in disallowed regions of the Ramachandran plot. The crystallographic data and refinement statistics are summarized in Table 1.

2.3. GEF activity

Single-turnover guanine-nucleotide exchange was measured using the fluorescence from a tryptophan residue in the switch II region of ARA7. Guanine nucleotide-exchange reactions were initiated by adding 100 µ*M* guanosine-5-(β,γ-imido)-triphosphate (GppNHp) to a solution consisting of 1 µ*M* ARA7-GDP in 20 m*M* Tris–HCl pH 8.0, 150 m*M* NaCl and 1 m*M* $MgCl_2$, 1 m*M* $CaCl_2$ or 1 m*M* EDTA at 298 K with 0.25–1 µ*M* VPS9a. Nucleotide exchange from GDP to GppNHp was detected as a decrease in intrinsic tryptophan fluorescence, reflecting a structural change around the switch II region of ARA7. Tryptophan was excited at 298 nm and emission was detected at 340 nm using a fluorescence spectrophotometer (F-2500, Hitachi High Technologies). Data were collected for 600 s following the addition of GppNHp.

2.4. Binding assay

The interaction between GST-VPS9a and ARA7 and the effects of metals and nucleotides were measured using surface plasmon resonance experiments (BIAcore 2000, BIAcore). Control GST or GST-VPS9a was immobilized on a CM5 Sensor Chip (BIAcore) using anti-GST antibodies. All data were collected in HBS-EP buffer consisting of 10 m*M* HEPES pH 7.4, 150 m*M* NaCl, 3 m*M* EDTA, 0.005% surfactant P20 or in HBS-Mg^{2+}-P buffer consisting of 10 m*M* HEPES pH 7.4, 150 m*M* NaCl, 1 m*M* $MgCl_2$, 0.005% surfactant P20. Rate constants for association (k_a) and dissociation (k_d) were calculated using the *BIAcore* software.

3. Results

3.1. Introducing a Ca^{2+} ion into the ARA7–VPS9a complex in the presence of nucleotides

Because our extensive attempts to introduce Mg^{2+} into ARA7-GDP–VPS9a crystals by soaking and cocrystallization failed, we evaluated other divalent metals that may be compatible with ARA7–VPS9a intermediates in the presence of nucleotides. The value of the dissociation constant K_d between ARA7-GDP and VPS9a was approximately 10^{-7} *M* in the absence of external nucleotides and metal ions (Table 2). The addition of 1 m*M* Mg^{2+} to the solution did not change the association and dissociation rate constants (k_a and k_d) or K_d significantly, suggesting that Mg^{2+} alone does not affect the binding of ARA7-GDP to VPS9a. Moreover, the addition of 1 m*M* GDP or GppNHp did not affect the binding constants. However, when 1 m*M* Mg^{2+} and 1 m*M* GDP or GppNHp were both present in the solution, no binding was observed between ARA7-GDP and VPS9a, suggesting destabilization of the ARA7–VPS9a complex. This observation implies that obtaining a stable complex of the ARA7-GDP-Mg^{2+}–VPS9a intermediate is difficult. The destabilizing effects of various nucleotides and Mg^{2+} were also measured using a surface plasmon resonance system. On the BIAcore sensor chip, we

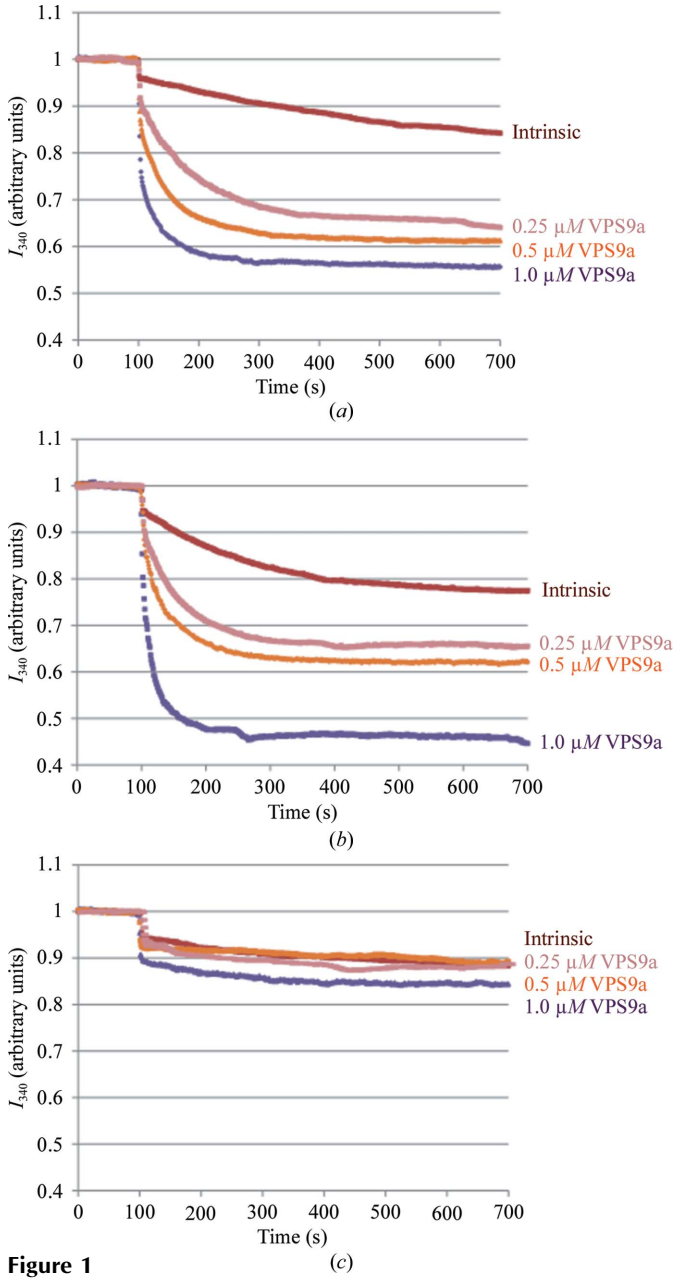

Figure 1
GEF activities in the presence of various divalent metals. GEF assays were performed in the presence of 1 m*M* $MgCl_2$ (*a*), 1 m*M* $CaCl_2$ (*b*) or 1 m*M* EDTA (*c*). Data were collected for 600 s following the addition of GppNHp.

expected a strong association between ARA7 and VPS9a because no nucleotide was present in the running buffer. Injecting GTP, GppNHp, GTPγS [guanosine 5′-*O*-(3-thiotriphosphate)], GDP or $GDPNH_2$ (aminophosphonic acid guanylate ester), but not GMP, onto the sensor chip resulted in immediate dissociation of ARA7 from immobilized VPS9a (Supplementary Fig. 1[1]), demonstrating that GTP and GDP destabilize the ARA7–VPS9a complex in the presence of Mg^{2+}.

We found that Ca^{2+} was less destabilizing towards the ARA7–VPS9a complex in the presence of nucleotides. The k_d value in the presence of 1 m*M* Ca^{2+} and 1 m*M* GDP was 6.3×10^{-2} s^{-1}, which is similar to the value obtained with 1 m*M* GDP and no metal ion (4.9×10^{-2} s^{-1}). Because a crystal was previously obtained using the latter condition (Uejima *et al.*, 2010), we hypothesized that Ca^{2+} could be introduced into the ARA7-GDP–VPS9a complex. To examine whether Ca^{2+} affects the GEF-catalyzed reaction, nucleotide-exchange assays were performed in the presence of 1 m*M* Mg^{2+}, Ca^{2+} or EDTA (Fig. 1). No significant difference in GEF activity was detected between Ca^{2+} and Mg^{2+}, whereas no exchange was observed in the presence of EDTA. Based on these results, we suspected that an ARA7-GDP–VPS9a intermediate containing Ca^{2+} would be as stable as the metal-free ARA7-GDP–VPS9a while retaining the ability to complete the guanine nucleotide-exchange reaction.

3.2. Coordination of the metal ion in the ARA7-GDP-Ca^{2+}–VPS9a intermediate

We were able to successfully crystallize the ARA7–VPS9a complex in the presence of GDP and Ca^{2+}, and the structure has a similar overall architecture to that of nucleotide-free ARA7-GDP–VPS9a (PDB entry 2efc) except for a structural rearrangement in VPS9a around the metal-binding region of ARA7 (Fig. 2; see below). Electron density was observed at the canonical Mg^{2+}-binding site and was judged to be a Ca^{2+} ion based on the seven coordinating atoms and their distances

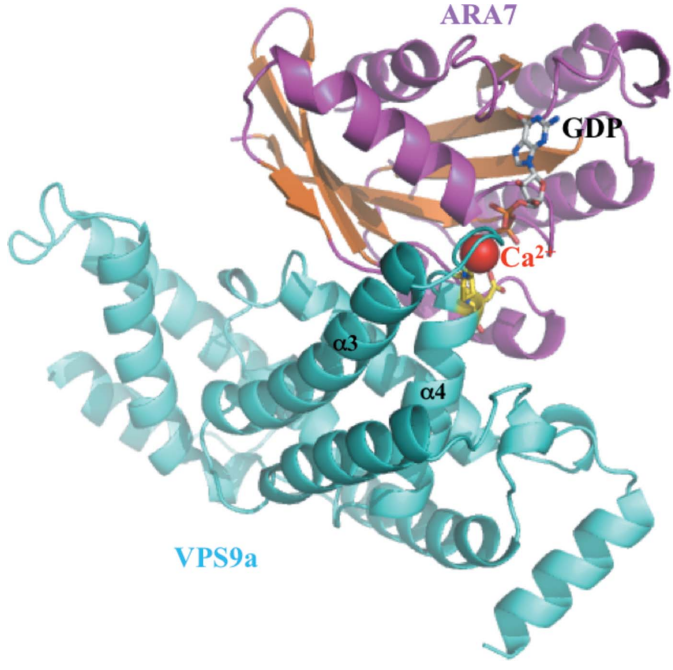

Figure 2
Structure of ARA7-GDP-Ca^{2+}–VPS9a. The structure of ARA7-GDP-Ca^{2+}–VPS9a is shown as a ribbon diagram. In the ARA7 molecule, α-helices and β-strands are displayed in orange and magenta, respectively. VPS9a is shown in cyan. GDP is drawn as a stick model to indicate C (grey), O (red) and P (orange) atoms. Ca^{2+} is represented as a red ball. Pro182 and Asp185 residues of VPS9a coordinating Ca^{2+} are shown as stick models with yellow C, red O and blue N atoms.

[1] Supplementary material has been deposited in the IUCr electronic archive (Reference: WD5196). Services for accessing this material are described at the back of the journal.

from the centre (range 2.3–2.5 Å; Fig. 3 and Supplementary Fig. 2*a*). In typical GTPases, the coordination number of Mg^{2+} is six, with distances of approximately 2.0 Å and a regular bipyramidal shape. The longer coordination distance for Ca^{2+} compared with Mg^{2+} allows more freedom in the number, lengths and angles of the coordination interactions (Harding, 2001). The crystallization conditions included 200 m*M* Ca^{2+}, suggesting that the binding metal was Ca^{2+}. The calcium bond-valence sum (CBVS) is 2.19, which is in good agreement with the expected value of 2.0 for calcium (Müller *et al.*, 2003). Moreover, an anomalous signal is observed in the anomalous difference electron-density map, confirming that the metal is Ca^{2+} rather than Mg^{2+} (Supplementary Fig. 2*b*). The seven coordinating O atoms are located on the β-phosphate of GDP, the side chain of the conserved Ser24 residue in the P-loop of ARA7, two VPS9a residues (the main chain of Pro182 and the side chain of Asp185) and three water molecules (Supplementary Fig. 2*a*). While coordination of the metal by GDP and the P-loop Ser24 is common to all isolated GTPases, coordination of the metal by the aspartate finger (Asp185) and the neighbouring main chain of Pro182 is the first example to be found in ARA7–VPS9a.

3.3. Structural differences between ARA7-GDP-Ca^{2+}–VPS9a and ARA7-GDP–VPS9a

Superposition of the ARA7-GDP-Ca^{2+}–VPS9a and ARA7-GDP–VPS9a structures (Fig. 4) showed that they are similar except for a slight tilt in ARA7 to make a metal-binding space open in the metal-bound complex compared with the direct contact between the aspartate finger of VPS9a and the GDP molecule in the metal-free complex. This tilt results from structural rearrangements in helices α3 and α4 of VPS9a and the loop between them (Fig. 4). In particular, the C-terminal region of α3 is bent by about 17° at Val165. This region and the following loop between two helices, α3 and α4 of VPS9a (Pro180–Glu186), are expected to be mobile, being characterized by higher temperature factors (Supplementary Fig. 3). A prominent shift was noted for Pro182 of VPS9a. The interaction between the main-chain carbonyl O atom of Pro182 and the Ca^{2+} requires the main-chain bond between Pro182 and Gly183 to flip in the metal-bound complex (Fig. 5). Another interesting shift was observed for direct interaction between the Ca^{2+} and the aspartate finger (Fig. 5). In the metal-free complex the aspartate finger forms a hydrogen bond to a β-phosphate O atom of GDP (3.1 Å) and an ionic interaction with the side-chain carboxyl of the P-loop Lys23 (2.8 Å). On the other hand, in the metal-bound complex the aspartate finger is located far away from the GDP (3.9 Å) and Lys23 of ARA7 (4.6 Å). The relative positions of GDP and the P-loop Lys23 are similar in the two complexes and the shift of the aspartate finger in the two intermediates is about 2.0 Å, indicating that the aspartate finger moves straight towards the P-loop Lys23 after the metal ion dissociates. In ARA7-GDP-Ca^{2+}–VPS9a the side chain of Glu186 of VPS9a forms a hydrogen bond to a water molecule (which may be a second Ca^{2+} ion bound to VPS9a; see §4), whereas this side chain is directed toward the canonical metal-binding site in ARA7-GDP–VPS9a (Fig. 5).

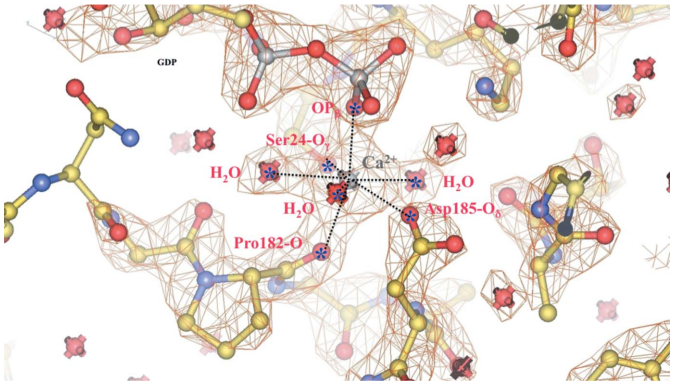

Figure 3
Electron-density map around the calcium-binding site. $2mF_o - DF_c$ electron-density map around Ca^{2+} contoured at 2σ. Seven coordinating O atoms, marked by asterisks, are observed around the Ca^{2+} ion, involving the β-phosphate of GDP, the side chains of Ser24 of ARA7 and Asp185 of VPS9a, the main chain of Pro182 of VPS9a and three O atoms from water molecules (also see Supplementary Fig. 2).

4. Discussion

4.1. Interaction between a divalent metal ion and the aspartate finger of VPS9a

The ARA7-GDP-Ca^{2+}–VPS9a complex structure reflects the earliest step in the GEF-mediated reaction (Supplementary Figs. 4 and 5), preceding the metal-free ARA7–VPS9a intermediates (Uejima *et al.*, 2010). Our previous attempt to

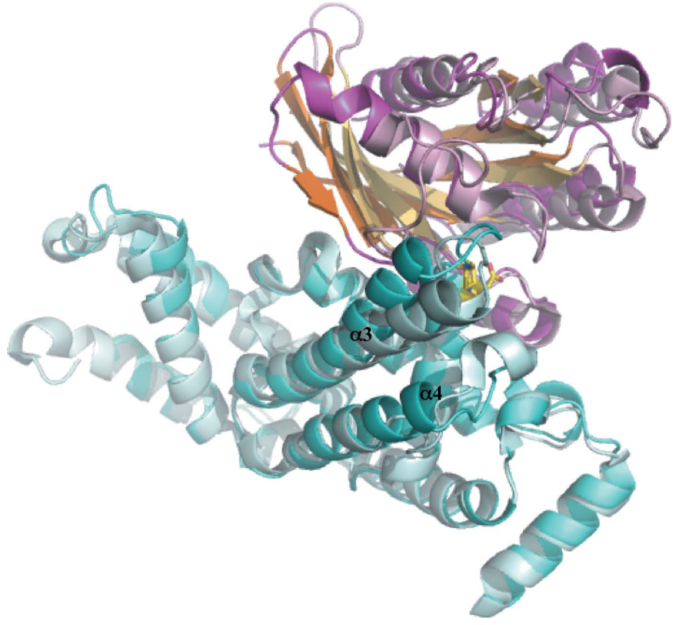

Figure 4
Superposition of the structures of ARA7-GDP-Ca^{2+}–VPS9a and ARA7-GDP–VPS9a. VPS9a of the ARA7-GDP-Ca^{2+}–VPS9a structure (colour-coded as in Fig. 2) is superimposed on that of the ARA7-GDP –VPS9a structure (α-helices and β-sheets of ARA7 are shown in light pink and yellow, respectively; VPS9a is shown in grey; PDB entry 2efc). GDP and Ca^{2+} are omitted from the figure for clarity.

model Mg^{2+} into metal-free ARA7-GDP–VPS9a resulted in steric interference between one of the Mg^{2+}-coordinating water molecules and the aspartate finger (Uejima *et al.*, 2010). In this report, we observed that the presence of both Mg^{2+} and GDP destabilizes the ARA7–VPS9a interaction, supporting the expected instability of the ARA7-GDP-Mg^{2+}–VPS9a intermediate. This instability of the complex makes it difficult to crystallize the earliest intermediate of the GEF-mediated reaction. To examine how ARA7-GDP-Mg^{2+} binds VPS9a and how the metal ion is excluded from the complex, we cocrystallized ARA7–VPS9a with Ca^{2+} and GDP. The structure demonstrates that Ca^{2+} induces conformational changes of the Pro180–Glu186 loop region of VPS9a compared with the metal-free complex. Unexpectedly, the aspartate finger of VPS9a directly interacts with the divalent metal ion. The main-chain carbonyl of Pro182 in VPS9a also binds to the Ca^{2+} ion and flips from its position in the metal-free complex.

Loss of Mg^{2+} reportedly weakens the binding affinity between the nucleotide and the GTPase by several orders of magnitude (Renault *et al.*, 2001; Vetter & Wittinghofer, 2001), and the removal of Mg^{2+} could be critical for GEF-catalyzed nucleotide exchange. However, in the ARA7-GDP-VPS9a intermediate (Uejima *et al.*, 2010) elimination of Mg^{2+} would not induce dissociation of GDP from the ARA7–VPS9a complex. Indeed, ARA7 purified without Mg^{2+} is in the fully GDP-bound form, indicating relatively strong binding between ARA7 and GDP. We observed that the aspartate finger electrostatically pulls the P-loop lysine of ARA7 away from the β-phosphate of GDP, which would enhance GDP release (Uejima *et al.*, 2010). Unexpectedly, the structure of the ARA7-GDP-Ca^{2+}–VPS9a intermediate suggests that the aspartate finger is also involved in the earlier step of the GEF-mediated reaction by recognizing the metal just after the binding of the substrate ARA7-GDP-Mg^{2+}. The ARA7-GDP-Ca^{2+}–VPS9a intermediate structure suggests how the aspartate finger destabilizes the metal binding.

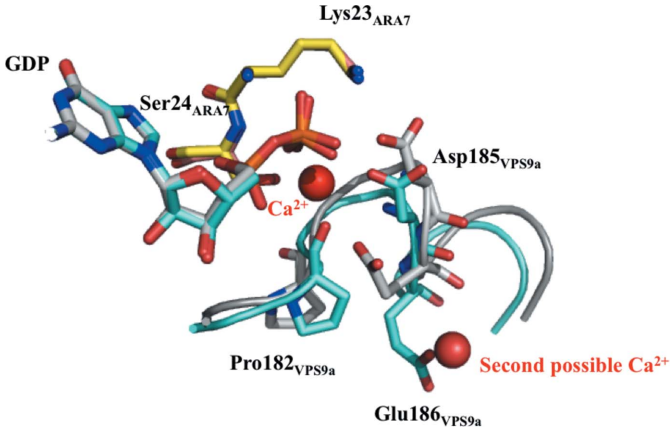

Figure 5
Nucleotide-binding and metal-binding sites in ARA7–VPS9a. The VPS9a main chains of the ARA7-GDP-Ca^{2+}–VPS9a and ARA7-GDP–VPS9a structures are shown in cyan and grey, respectively. The main-chain carbonyl of Pro182 flips and interacts with the Ca^{2+} in the ARA7-GDP-Ca^{2+}–VPS9a complex. Asp185 of VPS9a directly interacts with both Ca^{2+} and GDP in the ARA7-GDP-Ca^{2+}–VPS9a complex and with GDP in the ARA7-GDP–VPS9a complex. In the ARA7-GDP-Ca^{2+}–VPS9a complex Glu186 of VPS9a swings away from the metal-binding site towards the position of a water molecule at which a large density was observed (see Supplementary Fig. 6 and §4). The C atoms of GDP molecules are shown as cyan (ARA7-GDP-Ca^{2+}–VPS9a complex) and grey (ARA7-GDP-Ca^{2+}–VPS9a complex) sticks. The Ca^{2+} is represented by a red ball. The C atoms of the Lys23 and Ser24 residues of ARA7 are shown as magenta (ARA7-GDP-Ca^{2+}–VPS9a complex) and yellow (ARA7-GDP–VPS9a complex) sticks.

4.2. Proposed mechanism for release of the metal ion from ARA7–VPS9a

The structure of the ARA7-GDP-Ca^{2+}–VPS9a intermediate provides insights into the dissociation of Mg^{2+} from ARA7-GDP. In a hypothetical ARA7-GDP-Mg^{2+}–VPS9a intermediate, Mg^{2+} would also be recognized by the aspartate finger. However, the coordination of Ca^{2+} by seven ligands is partly incongruent with Mg^{2+} coordination. Moreover, the highly mobile region around Pro180–Glu186 of VPS9a would also be a disadvantage for Mg^{2+} coordination. The direct recognition of Mg^{2+} by the VPS9a aspartate finger may result in a more unstable environment for Mg^{2+} binding to ARA7-GDP compared with the case of Ca^{2+}.

As shown by Delprato and coworkers, the kinetics of guanine-nucleotide exchange vary among Rabs (Delprato *et al.*, 2004). Notably, several Rabs efficiently exchange guanine nucleotides in the presence of EDTA without GEF, whereas others require GEF. Rab5 seems to require GEF to maximize the exchange rate, yet the removal of Mg^{2+} should precede GDP release. Here, the aspartate finger recognizes the divalent metal of ARA7-GDP-Mg^{2+} and destabilizes the binding of the metal ion. After Mg^{2+} is removed, the aspartate finger binds the β-phosphate of GDP, which may serve to drive Mg^{2+} out of the complex.

GEFs of the *trans*-type, such as Vps9 and Sec7, use a catalytically critical acidic finger from the GEF rather than a hydrophobic alanine residue from the switch II region of the GTPase in a *cis* manner as observed for the Ras, Ran and Rho GTPases (Thomas *et al.*, 2007). VPS9a uses the aspartate finger to interact with and remove both the metal ion and GDP without the need for additional protein regions such as the WW motif in PRONE or the sensor valine in DOCK9 (Thomas *et al.*, 2007; Yang *et al.*, 2009).

Owing to the flexibility of the Pro180–Glu186 region of VPS9a, the reorganization of the main chain caused by the interaction between Ca^{2+} and the main-chain carbonyl of Pro182 could also occur with Mg^{2+}. In any case, after release of the metal ion the main chain of Pro182 flips back to restore the conformation observed in the ARA7-GDP–VPS9a intermediate (Fig. 5). The aspartate finger then binds the β-phosphate of GDP and Lys23 of ARA7 such that the aspartate finger pulls Lys23 away from the β-phosphate of GDP and hands Lys23 over to Asp65 of switch II in ARA7 (Uejima *et al.*, 2010). As a result, the rigid ionic interaction between the β-phosphate of GDP and Lys23 of ARA7 is weakened, and GDP is released from ARA7 to produce a nucleotide-free ARA7–VPS9a intermediate. In the nucleotide-free intermediate Lys23 of ARA7 is stabilized by an ionic interaction

with Asp65 and a hydrogen bond to the main-chain carbonyl of Thr66, two residues that are located in the conserved DTAGQE sequence of the ARA7 switch II region.

We previously suggested that GTP could be accommodated in the nucleotide-free binary Rab21–Rabex-5 complex (Uejima *et al.*, 2010). This model shows that the aspartate finger forms a hydrogen bond to the γ-phosphate of GTP, which is similar to the interaction between the β-phosphate of GDP and the aspartate finger in the ARA7-GDP–VPS9a intermediate. Mg^{2+} could also be recognized by the aspartate finger in a presumed ARA7-GTP-Mg^{2+}–VPS9a intermediate, as observed for the ARA7-GDP-Ca^{2+}–VPS9a intermediate.

4.3. The possibility of a second Ca^{2+} ion binding to Glu186 of VPS9a

In addition to the Ca^{2+} ion that binds in the canonical metal-binding site of the GTPase near GDP, we observed an electron-density peak located 2.4 Å away from the side chain of Glu186 of VPS9a (Supplementary Fig. 6*a*). The density is surrounded by five possible ligands (Glu186 and Asp125 of VPS9a and three water molecules) at distances of between 2.4 and 2.8 Å, suggesting that this density is a Ca^{2+} ion (Supplementary Fig. 6*b*). Although the CBVS value of 1.19 is lower than the expected value of 2.0 for calcium, a weak anomalous signal can be observed (Supplementary Fig. 2*b*). However, placing a Ca^{2+} ion at this position markedly increased the *B* factor (data not shown). Therefore, we placed a water molecule at this location in the final model. The side chain of Glu186 swings toward the canonical metal-binding site in the ARA7-GDP–VPS9a intermediate, as if Glu186 mediates two neighbouring metal-binding sites. Interestingly, not only the aspartate finger (Asp185) but also Glu186 are conserved in most Vps9 proteins. Such a second Ca^{2+}-binding site might provide a pathway for metal-ion removal or introduction.

Another pathway to remove the metal ion has been proposed for a complex between RhoA and the bacterial GEF mimic IpgB2. The GDP-bound and Mg^{2+}-bound RhoA–IpgB2 complex indicated that a shift of Mg^{2+} from the canonical metal-binding site to the α-phosphate of GDP led to release of the metal ion (Klink *et al.*, 2010). Thus, several different mechanisms to introduce and remove metal ions during GEF-catalyzed guanine nucleotide-exchange reactions may exist.

We thank the Photon Factory staff for encouragement, helpful discussions and assistance in data collection. This work was supported by Targeted Protein Research Program and a Grant-in-Aid for Scientific Research from the Ministry of Education, Culture, Sports, Science and Technology of Japan.

References

Barr, F. & Lambright, D. G. (2010). *Curr. Opin. Cell Biol.* **22**, 461–470.
Béraud-Dufour, S., Robineau, S., Chardin, P., Paris, S., Chabre, M., Cherfils, J. & Antonny, B. (1998). *EMBO J.* **17**, 3651–3659.
Boriack-Sjodin, P. A., Margarit, S. M., Bar-Sagi, D. & Kuriyan, J. (1998). *Nature (London)*, **394**, 337–343.
Buchwald, G., Friebel, A., Galán, J. E., Hardt, W. D., Wittinghofer, A. & Scheffzek, K. (2002). *EMBO J.* **21**, 3286–3295.
Cherfils, J. & Chardin, P. (1999). *Trends Biochem. Sci.* **24**, 306–311.
Delprato, A. & Lambright, D. G. (2007). *Nature Struct. Mol. Biol.* **14**, 406–412.
Delprato, A., Merithew, E. & Lambright, D. G. (2004). *Cell*, **118**, 607–617.
Emsley, P. & Cowtan, K. (2004). *Acta Cryst.* D**60**, 2126–2132.
Goh, T., Uchida, W., Arakawa, S., Ito, E., Dainobu, T., Ebine, K., Takeuchi, M., Sato, K., Ueda, T. & Nakano, A. (2007). *Plant Cell*, **19**, 3504–3515.
Goldberg, J. (1998). *Cell*, **95**, 237–248.
Harding, M. M. (2001). *Acta Cryst.* D**57**, 401–411.
Horiuchi, H., Lippé, R., McBride, H. M., Rubino, M., Woodman, P., Stenmark, H., Rybin, V., Wilm, M., Ashman, K., Mann, M. & Zerial, M. (1997). *Cell*, **90**, 1149–1159.
Itzen, A. & Goody, R. S. (2011). *Semin. Cell Dev. Biol.* **22**, 48–56.
Klink, B. U., Barden, S., Heidler, T. V., Borchers, C., Ladwein, M., Stradal, T. E., Rottner, K. & Heinz, D. W. (2010). *J. Biol. Chem.* **285**, 17197–17208.
Kraulis, P. J. (1991). *J. Appl. Cryst.* **24**, 946–950.
Laskowski, R. A., MacArthur, M. W., Moss, D. S. & Thornton, J. M. (1993). *J. Appl. Cryst.* **26**, 283–291.
Merritt, E. A. & Murphy, M. E. P. (1994). *Acta Cryst.* D**50**, 869–873.
Mossessova, E., Corpina, R. A. & Goldberg, J. (2003). *Mol. Cell*, **12**, 1403–1411.
Müller, P., Köpke, S. & Sheldrick, G. M. (2003). *Acta Cryst.* D**59**, 32–37.
Murshudov, G. N., Skubák, P., Lebedev, A. A., Pannu, N. S., Steiner, R. A., Nicholls, R. A., Winn, M. D., Long, F. & Vagin, A. A. (2011). *Acta Cryst.* D**67**, 355–367.
Otwinowski, Z. & Minor, W. (1997). *Methods Enzymol.* **276**, 307–326.
Renault, L., Guibert, B. & Cherfils, J. (2003). *Nature (London)*, **426**, 525–530.
Renault, L., Kuhlmann, J., Henkel, A. & Wittinghofer, A. (2001). *Cell*, **105**, 245–255.
Sayle, R. A. & Milner-White, E. J. (1995). *Trends Biochem. Sci.* **20**, 374–376.
Sprang, S. R. & Coleman, D. E. (1998). *Cell*, **95**, 155–158.
Stenmark, H. (2009). *Nature Rev. Mol. Cell Biol.* **10**, 513–525.
Thomas, C., Fricke, I., Scrima, A., Berken, A. & Wittinghofer, A. (2007). *Mol. Cell*, **25**, 141–149.
Ueda, T. & Nakano, A. (2002). *Curr. Opin. Plant Biol.* **5**, 513–517.
Ueda, T., Yamaguchi, M., Uchimiya, H. & Nakano, A. (2001). *EMBO J.* **20**, 4730–4741.
Uejima, T., Ihara, K., Goh, T., Ito, E., Sunada, M., Ueda, T., Nakano, A. & Wakatsuki, S. (2010). *J. Biol. Chem.* **285**, 36689–36697.
Vagin, A. & Teplyakov, A. (2010). *Acta Cryst.* D**66**, 22–25.
Vetter, I. R. & Wittinghofer, A. (2001). *Science*, **294**, 1299–1304.
Winn, M. D. *et al.* (2011). *Acta Cryst.* D**67**, 235–242.
Worthylake, D. K., Rossman, K. L. & Sondek, J. (2000). *Nature (London)*, **408**, 682–688.
Yang, J., Zhang, Z., Roe, S. M., Marshall, C. J. & Barford, D. (2009). *Science*, **325**, 1398–1402.
Zerial, M. & McBride, H. (2001). *Nature Rev. Mol. Cell Biol.* **2**, 107–117.